International Journal of Neural Systems, Vol. 0, No. 0 (2005) 1–16

ASSESSING FUNCTIONAL BRAIN NETWORK DYNAMICS IN DYSLEXIA FROM fNIRS DATA

NICOLÁS J. GALLEGO-MOLINA[1,4], ANDRÉS ORTIZ[1,4], FRANCISCO J. MARTÍNEZ-MURCIA[2,4], IGNACIO RODRÍGUEZ-RODRÍGUEZ[1], JUAN L. LUQUE[3]

[1]*Department of Communications Engineering, University of Malaga, 29071 Spain*

[2]*Department of Signal Theory, Networking and Communications, University of Granada, 18010 Spain*

[3]*Department of Developmental and Educational Psychology, University of Málaga, 29071 Spain*

[4]*Andalusian Research Institute in Data Science and Computational Intelligence, Spain*

E-mail: njgm@ic.uma.es

Developmental dyslexia is characterized by a deficit of phonological awareness whose origin is related to atypical neural processing of speech streams. This can lead to differences in the neural networks that encode audio information for dyslexics. In this work, we investigate whether there exist such differences using fNIRS and complex network analysis. We have explored functional brain networks derived from the low-level auditory processing of non-speech stimuli related to speech units such as stress, syllables or phonemes of skilled and dyslexic seven-year-old readers. A complex network analysis was performed to examine the properties of functional brain networks and their temporal evolution. We characterized aspects of brain connectivity such as functional segregation, functional integration or small-worldness. These properties are used as features to extract differential patterns in controls and dyslexic subjects. The results corroborate the presence of topological organizations discrepancies of functional brain networks and their dynamics that differentiate between controls and dyslexic subjects, reaching an AUC up to 0.89 in classification experiments.

Keywords: Network dynamics; functional connectivity; fNIRS; complex network analysis; Dyslexia.

1. Introduction

Children with Developmental Dyslexia (DD) are at risk for detrimental effects on self-esteem, depression and school failure. This learning disability affects 5%-12% of the world's population[1] hindering the learning process for the acquisition of reading skills, despite normal intelligence and educational opportunities. In this process, children base their learning on the correspondence of distinctive visual symbols with sound units (phonology).[2] The ability to recognize, identify, or manipulate any phonological unit within a word (phoneme, rime, or syllable) is named phonological awareness and is predictive of reading and spelling acquisition.[2] In most theories, DD is characterized by showing a phonological processing deficit across ages, languages and cultures. However, the biological causes and processes underlying DD are not well understood. Studying the causes of this phonological disorder may provide objective markers for a more precise and early diagnosis that lack the drawbacks of traditional diagnosis methods. Traditional assessment is specifically designed to measure the different behavioral variables involved in the reading process. They are designed for readers, limiting

the minimum age for an early diagnosis, and are frequently affected by exogenous variants. This results in delayed diagnosis and errors that can have a fundamental impact on the personal and intellectual development of affected children.[3]

Moreover, biomarker research offers valuable information to better understand the neural basis of DD. Several hypotheses have been proposed to explain the underlying cause of the phonological deficit. On the one hand, works as Refs. 4, 5, 6 attribute the phonological deficit to difficulties in the specific language processing domain. On the other hand, Goswami[7] proposed the Temporal Sampling Framework (TSF) attributing the phonological disorders to low-frequency phase locking mechanisms in auditory cortex. Other works take this hypothesis as a starting point, such as Refs. 8, 9, 10, 11, and regardless of the different methodological approaches, there is consensus that phonological difficulties originate in the atypical neural processing of speech streams.[7]

The speech signal contains information on different time scales that correspond to key phonological units: slow rhythmic prosody (0.5–1 Hz), syllable (4–8 Hz) and phoneme (12–40 Hz).[12] The brain encode this phonological structure (of speech rhythm) through neural entrainment of cortical oscillations at different preferred rates with temporal information in the speech signal.[13] This multi-time resolution analysis take place in cortical areas connected into networks that are themselves organized to support speech and language processing. The number and arrangement of these cortical regions demonstrate that the system is considerably more complex and distributed.[14] This paves the way for applying advances in complex network analysis to the study of neurobiological mechanisms that process speech and language, and to the neuroscience field in general.[15]

Many complex systems can be represented mathematically as a network consisting of a set of nodes and links. Complex network analysis offers valuable avenues to characterize brain networks. It uses measures from graph theory that are neurobiologically meaningful.[16] It allows the exploration of connectivity abnormalities of the brain processes in neurological and psychiatric conditions. In DD atypical auditory oscillatory activity is proposed to be a central mechanism. This would alter the involved brain functional network, impairing speech coding and yielding the phonological deficit that dyslexic children and adults exhibit.

There are several works that apply complex networks analysis to the study, exploration and diagnosis of DD. Ref. 17 examines the network topology of the phase synchronization connectivity in the recorded electroencephalograph (EEG) data from typical and dyslexic readers while listening to a random sequence of syllables and a series of trisyllabic real words. They noticed a more interconnected topology in the theta-band network in the right frontal site for word tracking in dyslexic readers. Other works[18–20] investigate the organization of functional connectivity networks from EEG of dyslexics and typical readers at rest and while performing an audiovisual task. They explore differences in the topological properties with graph metrics. A graph-theoretic approach have been employed in Ref. 21 to assess functional connectivity in DD while presenting a visual stimuli in an event-related EEG experiment. Ref. 22 use a stimulus-driven approach to test the TSF with the exploration and analysis of the functional connectivity from the speech processing network in magnetoencephalograph (MEG) signals. In Ref. 11 they analyze MEG signals recorded in an experiment in which spoken sentences were presented to dyslexic readers and age-matched controls. Then, they apply graph metrics to speech perception networks evidencing that abnormal neural entrainment and impaired connectivity within these networks are associated with phonological disorders in dyslexia. Ref. 23 performs a data-driven approach to study whole brain networks of functional magnetic resonance imaging (fMRI) functional connectivity in dyslexic versus typical readers. The authors of Ref. 24 investigate the use of graph metrics of functional connectivity that emerge throughout the reading network under different audiovisual task to predict reading difficulty. Recently we have presented a work where we explore brain coupling between frequency bands from EEG data to construct networks and apply graph theory analysis.[25] With this we investigate differences in the graph metrics between skilled readers and dyslexic children.

All these works use common data acquisition techniques as EEG, MEG and fMRI. However, we note the absence of the application of complex networks analysis to functional near-infrared spectroscopy (fNIRS) data in DD. This quiet, safe and non-invasive technique is particularly suitable for the

study of functional connectivity and brain networks in children.[26] fNIRS has practical advantages such as low operating costs, ease of application and tolerance to movement,[27] and has been used for experiments with children, infants, and adults. Ref. 28 explores brain functional connectivity in rest and sleep states, and Ref. 29 applies graph analysis to functional connectivity in prefrontal cortex of healthy adults. More related to our aim, Ref. 30 study the relationship between functional connectivity in children's reading networks and reading ability, and Ref. 31 explore fNIRS signals to investigate possible hemispheric asymmetry during speech processing in children with DD.

We propose the use of complex network analysis and functional connectivity via fNIRS for the exploration and diagnosis of DD. The study is based on an experiment with 57 seven year-old children, typical readers and dyslexics. The fNIRS signals were recorded while the participants were presented non-interactive auditory stimuli. These stimuli consist in amplitude modulated white noise at frequencies related to the phonological units of the Spanish language. We hypothesize that exploration and analysis of the functional brain networks thus originated will provide information and reveal characteristic patterns of DD. The remainder of the paper includes: First, in Section 2 we describe the database and methodology. In Section 3 we present the main results, and in Section 4, these are discussed and interpreted. Lastly, main conclusions are given in Section 5

2. Materials and Methods

2.1. *Database*

In this work we rely in a dataset provided by the LEEDUCA research group at the University of Málaga (Spain).[32] This dataset consists of 57 selected right-handed native Spanish speakers of seven years old, with no hearing impairments and normal or corrected-to-normal vision. The procedure to establish the 40 skilled readers of control group and the 17 dyslexic readers of experimental group was carried out according to the Special Education School Services (SESS) and following the standards.[33] All dyslexic children in this study had received a formal diagnosis of dyslexia at school. None of the skilled readers reported having reading or spelling difficulties or have received a prior formal diagnosis of dyslexia. The legal guardians of the participants understood the study, were present throughout the experiment, and gave written consent.

2.2. *fNIRS and Preprocessing*

fNIRS is a noninvasive method of extracting information of the brain by using near-infrared spectrum light in the range of 650–900nm.[34] In this range near-infrared light is relatively transparent to human tissues. However, it is absorbed by oxygenated hemoglobin (HbO) and deoxygenated hemoglobin (Hbr) in the human cortex. In our system a source emitted the light at two wavelengths 760Hz and 850Hz, for HbR and HbO respectively. fNIRS is based on the physiological principle of neurovascular coupling like fMRI. This concept describes the relationship between neuronal activity and localized changes in cerebral blood flow. Active neurons receive more oxygen from the blood than the inactive ones through a process called the hemodynamic response or the Blood Oxygenation Level–Dependent (BOLD) response. As in fMRI, an increase in HbO is an indicator of neuronal activity. In fNIRS this is followed by a a decrease in Hbr.

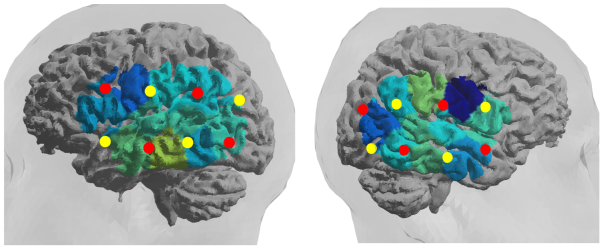

Figure 1. fNIRS optodes for left and right hemispheres. Sources are red and detectors yellow.

The equipment used for the fNIRS acquisitions was the NIRSport system with 16 optodes. The system consists of 8 sources, that emit the light, and 8 detectors. A source–detector pair makes up a channel, altogether we have 20 fNIRS channels. In Fig. 1 we can see the location of the optodes. These are placed over the language and auditory areas of the human brain. Fig. 2 shows the position of the optodes and channels in the EEG 10-20 system. For the left hemisphere, the sources were placed in the positions FC5, T7, CP5, P7, and detectors in FT7, C5, TP7,

P5. For the right hemisphere, sources were placed in FT8, C6, TP8, P6, and detectors in FC6, T8, CP6, P8 positions of the EEG 10-20 system. This provides information on which brain areas are acquired by the fNIRS channels. The fNIRS signals were recorded at 7.8Hz, while participants were exposed to auditory stimuli consisting of white noise modulated at 4.8, 16, and 40 Hz. Each stimulus had a duration of 2.5 minutes and was presented sequentially twice (4.8Hz-16Hz-40Hz and 40Hz-16Hz-4.8Hz) with a total duration of 15 minutes.

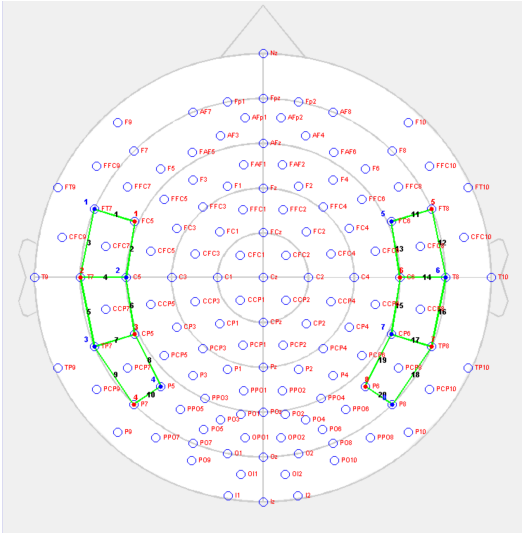

Figure 2. fNIRS channels and optodes with EEG 10-20 system. Sources are red, detectors blue, and channels are at the midpoint of each green line between a source-detector pair.

Acquired signals were then preprocessed using the python library MNE-Python,[35] MNE-NIRS[36] and nirsLAB (`www.nitrc.org`). Fig. 3. shows an overview of the fNIRS preprocessing pipeline. First, we interpolate the detectors saturation and convert the intensity to optical density. Then, we apply Temporal Derivative Distribution Repair (TDDR) to correct the motion artifacts of the optical density signal.[37] This method does not require any tuning parameters to efficiently remove baseline shift and spike artifacts.

We transform the raw signal to hemoglobin concentration applying the modified Beer–Lambert law[38] that uses an effective path length to account for light scattering and optical path length as it propagates through the tissue[39] as:

$$\Delta OD^{\lambda} \cong (\sum_{i} \epsilon_i^{\lambda} c_i) \cdot L \cdot PPF^{\lambda} \qquad (1)$$

where the effective pathlength is approximated by the product of an scaling factor to consider the part of the path that belongs to the brain called the Partial Pathlength Factor (PPF) and the distance along the surface between a source–detector pair (L); ΔOD^{λ} is the variation in optical density in an fNIRS channel, ϵ_i^{λ} is the extinction coefficient for a wavelength (λ) and the i^{th} chromophore (HbO or Hbr in fNIRS), and c_i is the chromophore concentration.

We filter the hemoglobin concentration signals with cutoff frequencies of 0.01Hz and 0.2Hz removing artifacts of heart rate and breathing from the hemodynamic response. Then, we extract epochs related to each stimuli and apply baseline correction. In this way, we have separated the stimuli for each subject. Finally, each stimulus is segmented into 25s temporal segments to explore the evolution of the hemodynamic response. The stimuli have a duration of 150s, resulting in a total of six temporal segments.

2.2.1. *Functional connectivity*

Functional connectivity is calculated by computing Spearman correlation coefficient for the hemoglobin concentration time series. We have measured this correlation coefficient for every fNIRS channel. This results in a set of 20×20 connectivity matrices, M_c, for HbO and HbR data. Fig. 4.a show an example of a connectivity matrix with the Spearman correlation coefficient between fNIRS channels. We have six connectivity matrices for each stimulus, representing the temporal evolution of functional connectivity in the hemodynamic response.

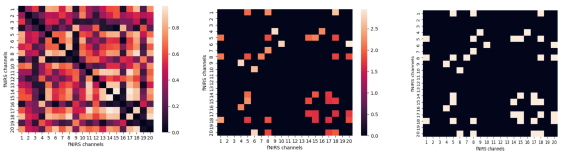

Figure 4. fNIRS connectivity matrices. a) Spearman correlation coefficient. b) Z-score connectivity matrix. c) Binanrized connectivity matrix

Surrogate permutation testing has been used to assess the significance of the connections measured.[40]

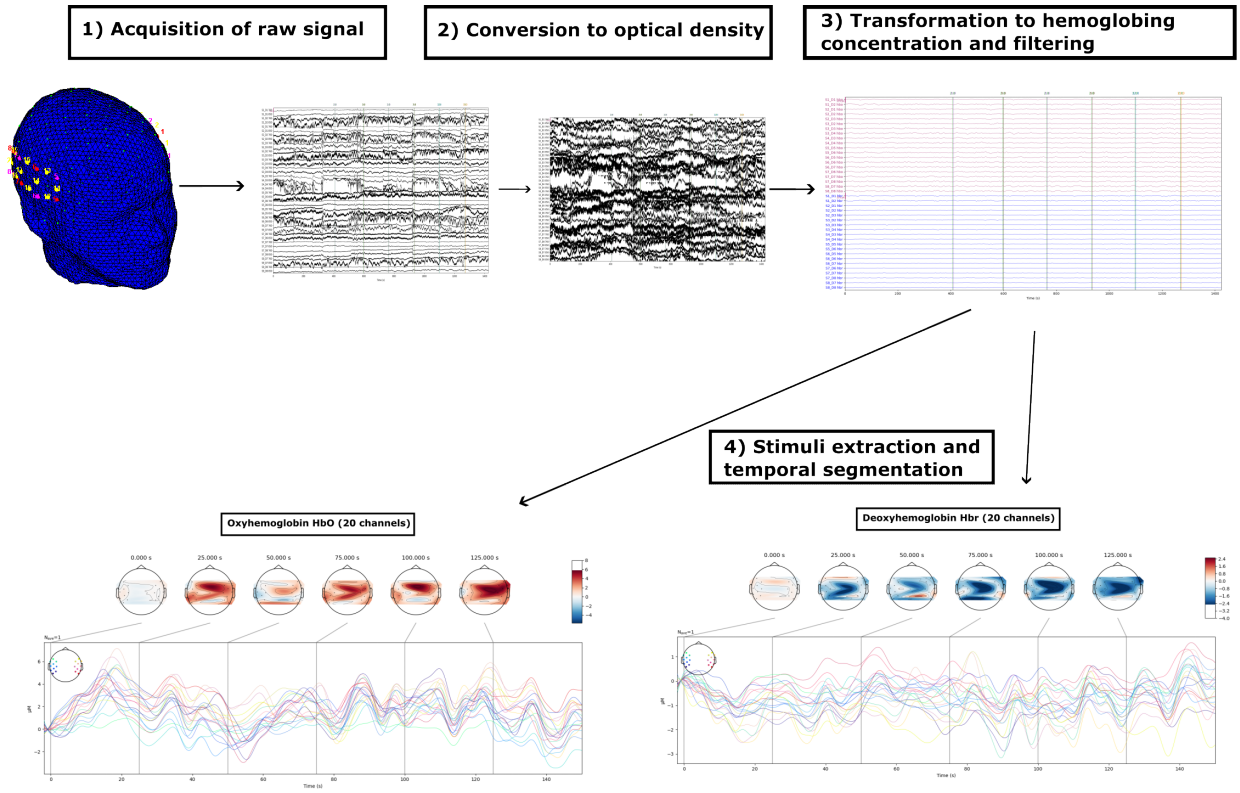

Figure 3. Schema of the overall fNIRS preprocessing. 1) Acquisition of raw intensity signals. 2) Conversion to optical density. 3) Transform the signal to hemoglobin concentration. 4) Extraction of stimuli and temporal segmentation.

We approximate the null distribution by computing for each connectivity matrix 1000 surrogate connectivity matrices, M_{sur}. This is done by calculating the Spearman correlation coefficient between surrogates of the hemoglobin concentration time series. These surrogates are computed by swapping time blocks of the original signal. Then, we obtain a Z-score connectivity matrix, M_z, where each position indicates the significance of the connection (Spearman correlation coefficient) calculated with the original hemodynamic time series. We use the absolute values greater than 0.8 of the correlation coefficient and we calculate the Z-score connectivity matrix as

$$M_z = \frac{M_c - \mu_{sur}}{\sigma_{sur}} \tag{2}$$

where μ_{sur} is the mean of M_{sur} and σ_{sur} is the standard deviation of M_{sur}. From this significance matrix we select the ones with $Z - score > 1.65$, equivalent to a $p - value < 0.05$. Fig. 4.b represents the corresponding Z-score matrix of Fig. 4.a. Then, we binarize the Z-score connectivity matrices denoting the presence, 1, or absence, 0, of significant connections as we can see in Fig. 4.c.

2.3. *Complex Network Analysis*

We use the resulting binarized Z-score connectivity matrices (as in Fig. 4.c) to construct our brain networks. Graph theory is the natural framework to study and measure complex networks.[41] Each row and column from these matrices designate the nodes -fNIRS channels-, and matrix entries the links. Each link represents the presence of a significant functional connectivity between the hemodynamic time series of a fNIRS channel pair. These connectivity matrices are symmetrical, thus we use the lower triangular to construct the networks. As a result, we have networks represented by undirected and unweighted graphs as shown in Fig. 5. Thus, our networks have $N = 20$ nodes and K links depending on the connectivity matrix.

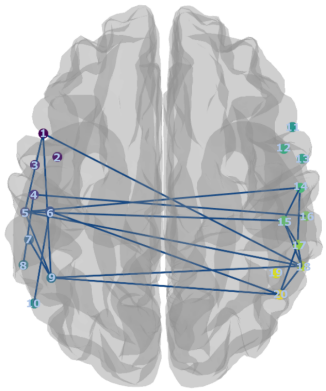

Figure 5. fNIRS network from matrix in Fig. 4 c)

These networks have properties that help us characterize aspects of brain connectivity. In our case, functional connectivity between fNIRS channels. Graph-theoretic approaches provide measurements to quantify how a network is connected. This network measurements are tools to understand and explore functional brain networks. It reveals properties of the underling networks derived from the activity over time of brain cognitive processes. A network measure characterize atributes of integration and segregation, test the resilience of networks, and evaluate the relevance of brain regions.[16]

An important measure is the node degree. It is the number of links connected to that node, and is computed as:

$$k_i = \sum_{j=1}^{N} a_{ij} \tag{3}$$

where a_{ij} is an entry for the connectivity matrix and k_i is the i^{th} node degree. This basic characteristic of the network can influence other more sophisticated network measures to be defined below.

2.3.1. *Functional segregation*

First, we will describe measures of functional segregation. This characteristic refers to the capacity of different brain regions to perform specialized processing,[16] quantifying the presence of clusters or modules in the network (Fig.6), and indicate segregated neural processing. The base measure is the number of triangles in the network. A triangle, t_i, is formed by sets of three nodes each of which is connected to each of the others[42]

$$t_i = \frac{1}{2} \sum_{j,h=1}^{N} a_{ij} a_{ih} a_{jh} \tag{4}$$

and for an individual node, we can measure the clustering coefficient (C_i) as the quantity of connected triangles among its neighbors.[43] The mean clustering coefficient, C, denotes the rates of clustered connectivity around individual nodes in a network

$$C = \frac{1}{N} \sum_{i=1}^{N} C_i \tag{5}$$

where C_i is the clustering coefficient of node i. A related measure that is normalized and unaffected by low-degree nodes is the transitivity of the network (T):

$$T = \frac{\sum_{j,h=1}^{N} 2t_i}{\sum_{j,h=1}^{N} k_i(k_i - 1)} \tag{6}$$

Other measures of segregation used are based on the community structure, which are clusters of nodes that have the maximum number of connections among themselves and the minimum number of connections between other groups (Fig. 6).[16] These metrics describe the size and composition of the interconnected groups of regions. This is quantified by the modularity (Q) computed by subdividing the network into communities[42]

$$Q = \sum_{u \in N} [e_{uu} - (\sum_{v \in M} e_{uv})^2] \tag{7}$$

where Q is a set of nonoverlapping communities, and e_{uv} the fraction of the total number of edges connecting the community u with the community v.

2.3.2. *Functional integration*

The brain must complement this ability to segregate the information processing and specialized computations in local circuits with the capacity to integrate specialized information from distributed brain regions.[44] This is known as functional integration, and use paths (Fig. 6) to characterize the communication of brain regions. It is necessary to note that functional connectivity paths cannot be directly associated to information flow on anatomical connections.[16] This is due to the statistical origin of functional connectivity path. A common measure of functional integration is the characteristic path length

of the network (L). It is the average shortest path length between all pairs of nodes in the network[43]

$$L = \frac{1}{N}\sum_{i=1}^{N} L_i \tag{8}$$

where L_i is the average distance between node i and all other nodes. The average inverse shortest path length between node i all other nodes j of the network is the node efficiency (E_i)[45]

$$E_i = \frac{1}{(N-1)}\sum_{j=1}^{N}\frac{1}{d_{ij}} \tag{9}$$

where d_{ij} is the shortest path length between node i and node j. The average efficiency of the network is known as the global efficiency (E_{glob}) and is proportional to the average inverse shortest path length of the nodes in the network.

$$E_{glob} = \frac{1}{N}\sum_{i=1}^{N} E_i \tag{10}$$

This measure denotes how efficient is the parallel information transfer in the network, making it a superior measure of integration.[46] Here we can define the local efficiency (E_{loc}) as the average efficiency of the local subgraphs of the network

$$E_{loc} = \frac{1}{N_{G_i}(N_{G_i}-1)}\sum_{j,k\in G_i}\frac{1}{d_{jk}} \tag{11}$$

where G_i is a subgraph formed by N_{G_i} nodes that are each directly connected to the node i. E_{loc} is applied as a measure of segregation. Since the node i does not belong to G_i, E_{loc} also measure the fault tolerance by quantifying the communication efficiency when the node i is removed.[45,46]

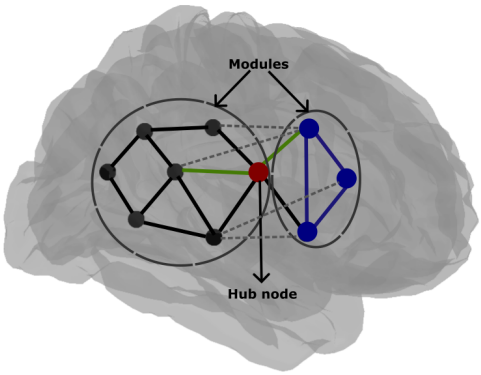

Figure 6. Illustration of network measures. The decomposition into modules (circles) and triangles (blue) are the base for measures of functional segregation. The shortest path lengths (green) are used for measures of integration. If we increase the network integration by adding the dashed links, the modules tend to disappear and the network segregation is reduced. Hub nodes (red) are part of a large number of short paths.

2.3.3. *Small-world networks*

There is evidence that functional brain networks are capable of rapid and real-time integration of information (functional integration) across segregated efficient brain regions (functional segregation).[47] This is due to a small-world organization of the networks, characterized by being significantly more clustered than random networks and having similar characteristic path length.[43] Ref. 48 proposed a measured of the small-worldness, S,

$$S = \frac{\gamma}{\delta} = \frac{\frac{C}{C_{rand}}}{\frac{L}{L_{rand}}} \tag{12}$$

where L_{rand} and C_{rand} are measures for the equivalent random graph, and L is the average shortest path length and C is the clustering coefficient of the original network. There is a small-world organization if $L \geq L_{rand}$ and $C \gg C_{rand}$, likewise, if $S > 1$.

2.3.4. *Centrality*

Small-world topology are also related with the abundance of hubs: influential brain regions (nodes) that exchange information with a high number of regions facilitating functional integration (Fig. 6).[16] The importance of individual nodes to be considered as hubs is evaluated with centrality measures. An usual measure of centrality is the nodal degree. Other measures are closeness centrality (CC) and betweenness centrality (BC). The former is, for each node, the inverse of the average shortest path length to all other nodes,[49] and the latter the proportion of all shortest paths that cross a particular node.[16]

2.3.5. *Network resilience*

Finally, we can characterize the network resilience, i.e., the network capacity to withstand disturbed brain function. A convenient measure is the assortativity coefficient (r),[50] it is usually quantified by a correlation coefficient between the number of links of the nodes. A positive assortativity coefficient indicate that the network is resilient to the removal of

high-degree hubs, since these hubs tend to be clustered together in an interconnected core. In a network with a negative assortativity coefficient, these hubs are broadly distributed over the network, which makes the network vulnerable to the removal of a high-degree hub. Other measure related to assortativity is the average neighbor degree that is computed on individual nodes.[51]

$$k_{nn,i} = \sum_{j=1}^{N} \frac{a_{ij} k_j}{k_i} \tag{13}$$

2.4. *Classification*

These network measurements have direct application in quantifying differences between the functional brain networks of patient groups and appropriate comparison groups.[15] Here, we consider networks measurements as features with potential diagnostic capability. We have measures from brain networks of controls and dyslexics over six temporal segments and three stimuli. In each stimulus we aggregate the measures of the temporal segments. Then, we use a Support Vector Machine classifier (SVC)[52] to assess the diagnostic accuracy of these features while taking into account the sensitivity-specificity trade-off.

The classification is performed in each stimulus as follows (Fig. 7). First, we construct datasets with the features from the functional brain networks measures using control and dyslexic subjects. We have a dataset for each feature (Clustering coefficient, transitivity, characteristic path length,..), and datasets for the combination of two, three and four features. Then, a stratified 5-fold cross-validation is used to split the dataset into train and test sets that change in each iteration. With this scheme, we train an SVC and estimate the performance.

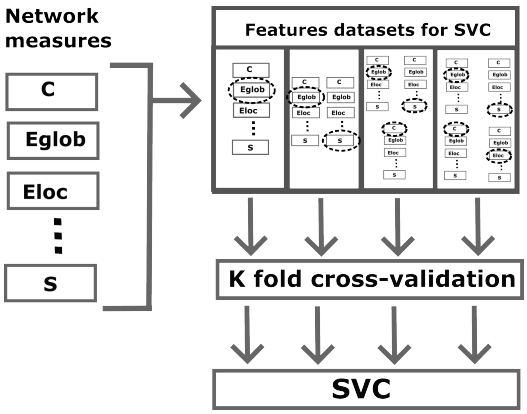

Figure 7. Schema of proposed classification methodology. We have four datasets with features from the functional brain networks measures of control and dyslexic subjects. The classification is performed by using one feature, the combination of two, three and four features. A stratified five-fold cross-validation is used.

3. Results

Complex network analysis provides features for the study and diagnosis of DD. To achieve this, an exploratory analysis of fNIRS signals and functional connectivity is essential. Once fNIRS signals have been processed, we examine them. First, we explore the average HbO and Hbr signals for control and dyslexic groups. We examine the temporal evolution for each stimulus separately, considering the mean between the first and second exposure of each stimulus to enhance the quality of the acquired signal. Fig. 8 shows a comparison of the HbO and Hbr signals for the three stimuli between control and dyslexic groups. We can see the mean hemoglobin concentration of each fNIRS channel and the topographic representation of the hemodynamic response at the beginning of each of the six temporal segments.

Once the stimulus signals have been explored, we analyze the functional connectivity in the fNIRS signals. Before investigating the development of connectivity in time segments, a result that provides valuable information is the globally significant connectivity matrices. These matrices are obtained following the procedure described in Sec. 2 and by merging the results of all the subjects in two sets, one for controls and another for dyslexics. We use aggregated surrogate matrices to obtain the significant connections of each group. This way, in Fig. 9 we can see the global Z-score connectivity matrices for each stimuli. These matrices show the significant connections with a Z-score greater than 1.65. Fig. 9 also shows the corresponding networks for HbO and Hbr signals in control and dyslexic groups. We can distinguish that there is more significant connections for dyslexia in all three stimuli, and that it presents interconnectivity between hemispheres. There is a common connectivity pattern between fNIRS channels 17, 18, 19 and 20, which derives from the source-detector pairs in the EEG 10-20 position of CP6, TP8, P6, P8.

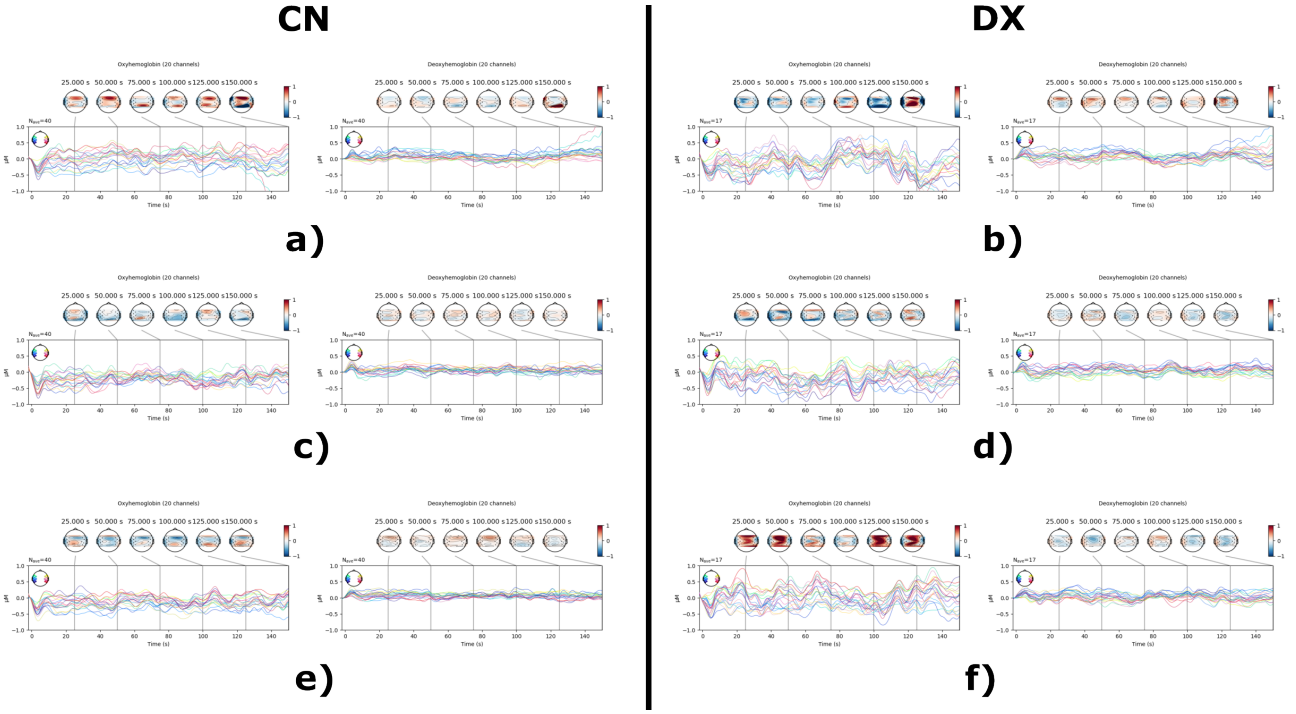

Figure 8. Average hemoglobin response for control and dyslexic groups. In each graph, the mean hemoglobin concentration of each fNIRS channel is represented and the topographic representation of the hemodynamic response at the beginning of each temporal segment. Each row corresponds to one stimulus: a) and b) 4.8Hz. c) and d) 16Hz. e) and f) 40Hz.

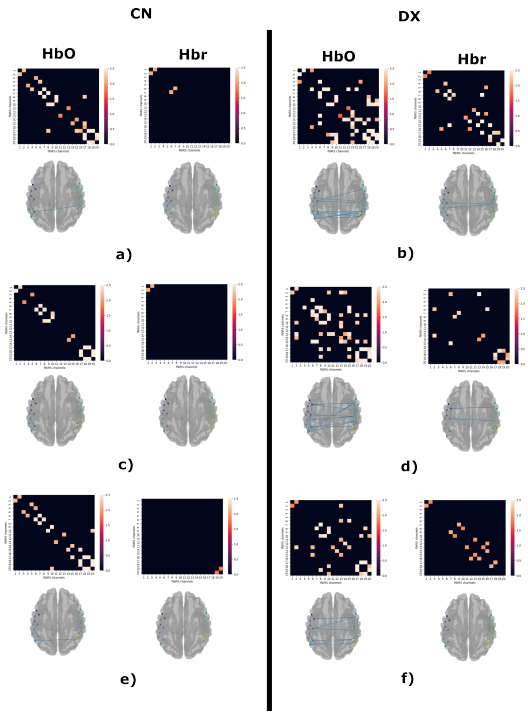

Figure 9. Global Z-score connectivity matrices and networks. a) and b) 4.8Hz. c) and d) 16Hz. e) and f) 40Hz.

3.1. *Complex Network Analysis Results*

We have employed complex network analysis to explore the development of functional connectivity in time segments. The connectivity matrices have been computed for each subject as described in Sec. 2.2.1. Then, with the binarized matrices, we construct a network for each temporal segment with the significant connections. We analyze the properties of these networks using graph measures that reveal features derived from functional connectivity of the underlying brain processes.

We present some of the network measurements used that are easier to interpret and make possible the analysis of network properties such as functional integration and segregation. In Fig. 10 we can see a comparison between global network metrics of control and dyslexic groups with the metrics of an ensemble of null-model networks generated with matched random networks.[53]

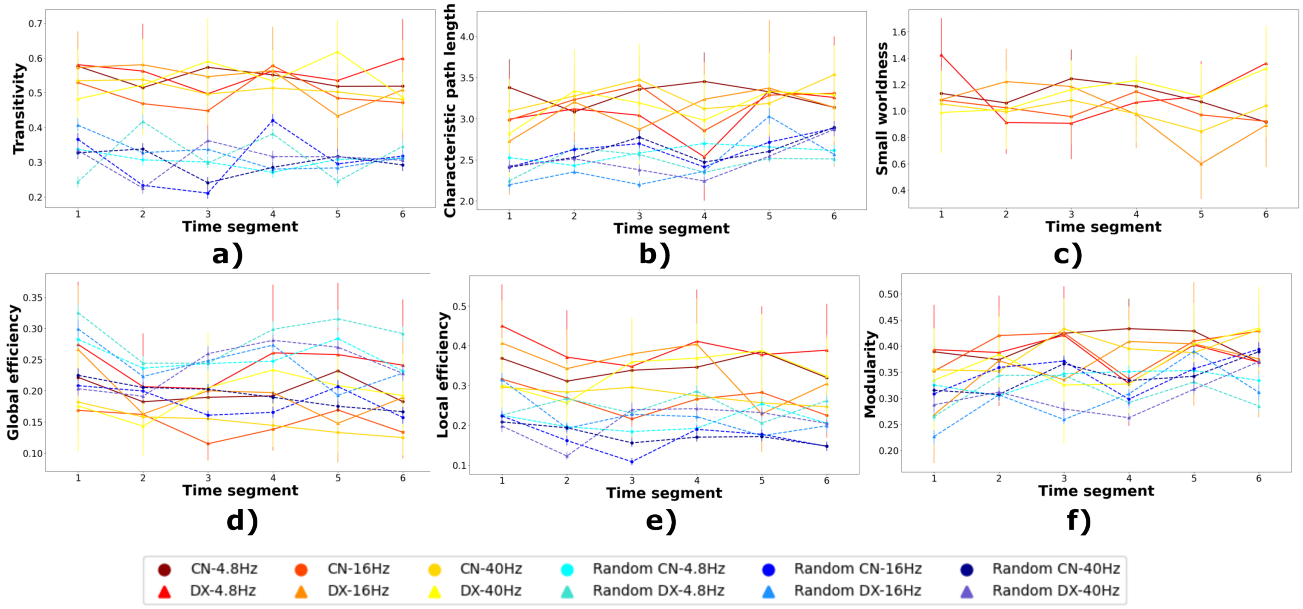

Figure 10. Global network metrics in the six temporal segments for control and dyslexics groups compared with the metrics of a null-model from an ensemble of 1000 matched random networks in each stimulus. a) Transitivity. b) Characteristic path length. c) Small-worldness. d) Global efficiency. e) Local efficiency. f) Modularity.

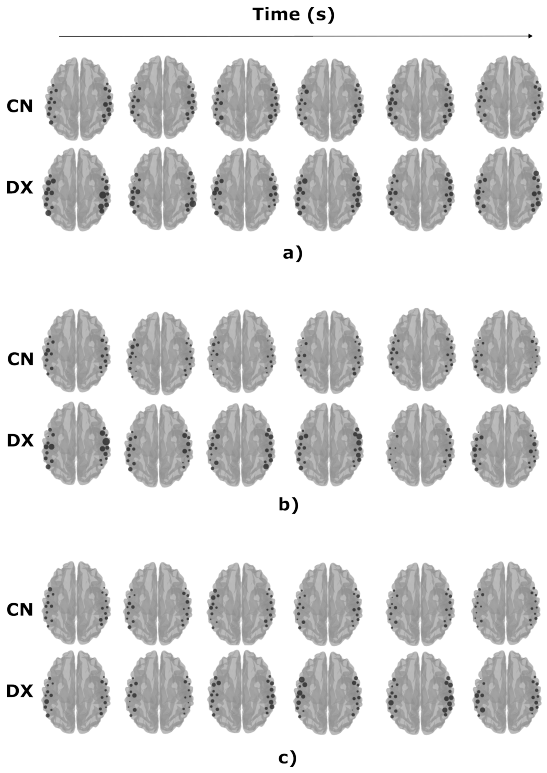

Figure 11. Mean clustering coefficient in each node for controls and dyslexics. a) 4.8Hz b) 16Hz c) 40Hz.

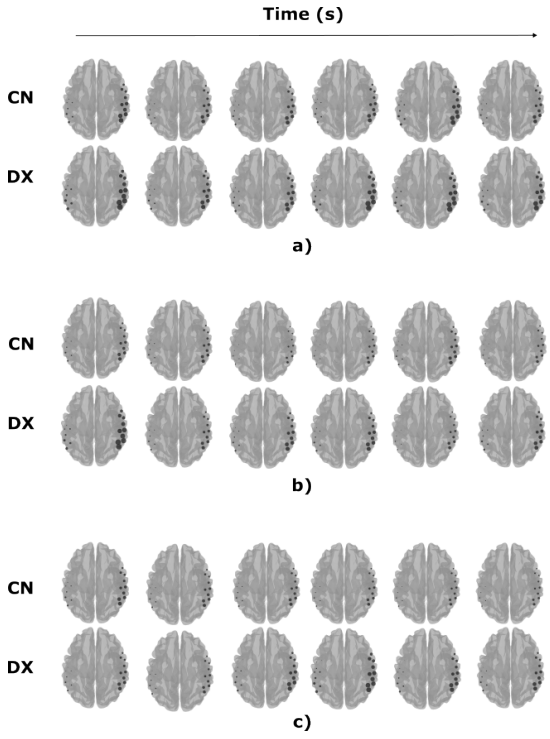

Figure 12. Mean nodal efficiency for controls and dyslexics. a) 4.8Hz b) 16Hz c) 40Hz.

Fig. 11 shows the clustering coefficient in each

node. This is the mean value for control and dyslexic groups, and the size of the node increases proportionally to the clustering coefficient. In the same way, Fig. 12 represents the mean nodal efficiency of the networks for each segment. In these figures we can examine the evolution of these measures comparing controls and dyslexics for each stimulus. In Fig. 11 we can observe that there is an increase of the clustering coefficient in the nodes of the dyslexic networks, and the greatest mean value is found in the first segments of the 4.8Hz and 16Hz stimuli. Fig. 12 shows greater mean values for the right hemisphere in both groups, with an intensification of node efficiency for dyslexics.

3.2. *Classification Results*

The classification is performed with the network measures as features. Thus, revealing that the properties of the fNIRS functional connectivity networks from the three stimuli entail differences between controls and dyslexics with a diagnostic capacity. Table 1 presents the classification results for the three stimuli, HbO and Hbr. This table shows the best SVC accuracy, sensitivity, specificity and Area Under ROC Curve (AUC) for one, two, three and four network features. Table 1 indicate the performance achieved by the SVC in a five-fold cross-validation scheme.

The results reported better performance for the networks from the HbO signals in 4.8Hz stimulus, and for Hbr in 16Hz and 40Hz. We pick the best classification result for each stimulus to evaluate the classification accuracy obtained. In each stimuli we have:

- small-worldness and local efficiency for 4.8Hz,
- clustering coefficient, local efficiency and betweeness centrality for 16Hz,
- local efficiency, modularity, nodal efficiency and assortativity coefficient for 40Hz.

We use permutation tests with a null distribution drawn from 1000 labels permutations. This is done in a five-fold cross-validation, in which we take as null hypothesis that there is no relationship between features and labels. With this, we evaluate such data-label link established by the classifier. Fig. 13 shows the performance achieved by the classifier with the random datasets in each permutation and the accuracy with the original dataset. It also displays the p-value calculated as the fraction of classification results where equal or better performance is achieved with the random datasets than with the original one.

4. Discussion

In this work we have combined fNIRS data and complex network analysis to investigate the neural entrainment to amplitude modulated white noise at 4.8Hz, 16Hz and 40Hz in Spanish children for DD diagnosis. These are three core speech units in Spanish: 4.8Hz stimulus for syllables, 16Hz stimulus for the intra-syllabic rhythms, and 40Hz stimulus for phonemes. We have used fNIRS signals to explore the functional brain connectivity of typical and dyslexic seven-year-old readers. Importantly, we merged this with a graph theory analysis of the resulting functional brain networks.

Our results support the idea that an atypical neural sampling of auditory signals underlies DD.[8,54,55] We have used a SVC to assess the diagnostic capability of measures from brain complex networks in DD. This classification use these measures as features, proving the existence of a link between the properties of functional brain connectivity networks and the neural sampling of auditory signals in typical readers and DD. Table 1 indicates that the best classification result is obtained using network features derived from the 40Hz stimulus, achieving an AUC of 0.89. This stimulus mimics the rate of phonemes in Spanish, where works as Ref. 13, 10, 54 have found a rightward synchronization asymmetry for the dyslexic group, driven by an atypical synchronization enhancement in the right auditory cortex. Our classifier has also achieved an AUC above 0.85 for the 4.8Hz stimulus. This is in line with Ref. 7, 10, where the deficit in encoding phonological information also occurs in the slow rhythms as proposed by the TSF. Both results sustain the hypothesis that the phonological deficit in dyslexia arises from an auditory deficit in neural entrainment to the low-frequency syllabic rate that hinders the next steps of phonological processing, where phonemes are processed.[11]

The classification results stem from the use of network measures through temporal segments as features to train an SVC. Network measures characterize the functional brain networks obtained from fNIRS signals, helping to understand and reveal properties of the underlying brain connectivity pro-

Table 1. Classification results with stratified K-fold cross-validation (five-folds)

Stimulus	Hemoglobin type	Features	Acc	Sens	Spec	AUC
	HbO	S	0.845 ± 0.097	0.65 ± 0.226	0.925 ± 0.1	0.835 ± 0.158
	HbO	**S, $\mathbf{E_{loc}}$**	$\mathbf{0.842 \pm 0.103}$	$\mathbf{0.7 \pm 0.267}$	$\mathbf{0.9 \pm 0.094}$	$\mathbf{0.856 \pm 0.147}$
	HbO	S, E_{glob}, Q	0.726 ± 0.203	0.75 ± 0.247	$0.7 \pm .359$	0.81 ± 0.144
4.8Hz	HbO	S, E_{glob}, Q, r	0.715 ± 0.234	0.833 ± 0.211	0.675 ± 0.359	0.825 ± 0.145
	Hbr	T	0.583 ± 0.133	0.583 ± 0.269	0.575 ± 0.302	0.669 ± 0.203
	Hbr	L, E_{loc}	0.58 ± 0.21	0.533 ± 0.452	0.575 ± 0.472	0.654 ± 0.093
	Hbr	T, L, BC	0.552 ± 0.181	0.533 ± 0.452	0.525 ± 0.45	0.587 ± 0.05
	Hbr	C, L, E_{glob}, E_{loc}	0.57 ± 0.201	0.6 ± 0.389	0.525 ± 0.435	0.654 ± 0.085
	HbO	Q	0.579 ± 0.12	0.617 ± 0.393	0.575 ± 0.17	0.538 ± 0.134
	HbO	T, E_{glob}	0.598 ± 0.151	0.667 ± 0.365	0.55 ± 0.322	0.619 ± 0.162
	HbO	T, E_{glob}, Q	0.615 ± 0.17	0.5 ± 0.447	0.65 ± 0.374	0.554 ± 0.16
16Hz	HbO	C, E_{glob}, E_{loc}, Q	0.562 ± 0.137	0.567 ± 0.389	0.55 ± 0.302	0.604 ± 0.136
	Hbr	C	0.806 ± 0.04	0.7 ± 0.041	0.85 ± 0.05	0.79 ± 0.065
	Hbr	C, E_{glob}	0.826 ± 0.051	0.667 ± 0.183	0.9 ± 0.094	0.792 ± 0.04
	Hbr	**C, $\mathbf{E_{loc}}$, BC**	$\mathbf{0.842 \pm 0.067}$	$\mathbf{0.717 \pm 0.163}$	$\mathbf{0.9 \pm 0.094}$	$\mathbf{0.79 \pm 0.074}$
	Hbr	C, E_{loc}, Q, BC	0.808 ± 0.029	0.7 ± 0.041	0.85 ± 0.05	0.806 ± 0.075
	HbO	E_{glob}	0.718 ± 0.147	0.483 ± 0.343	0.825 ± 0.127	0.652 ± 0.209
	HbO	E_{glob}, E_{loc}	0.614 ± 0.204	0.6 ± 0.327	0.6 ± 0.33	0.625 ± 0.247
	HbO	L, Q, E_i	0.636 ± 0.183	0.567 ± 0.389	0.65 ± 0.33	0.696 ± 0.216
40Hz	HbO	T, L, E_i, r	0.617 ± 0.149	0.567 ± 0.389	0.625 ± 0.323	0.673 ± 0.215
	Hbr	E_i	0.741 ± 0.23	0.683 ± 0.367	0.75 ± 0.387	0.86 ± 0.111
	Hbr	CC, r	0.839 ± 0.106	0.7 ± 0.267	0.9 ± 0.094	0.877 ± 0.105
	Hbr	E_{glob}, E_i, r	0.858 ± 0.111	0.683 ± 0.367	0.925 ± 0.1	0.892 ± 0.102
	Hbr	**$\mathbf{E_{loc}}$, Q, $\mathbf{E_i}$, r**	$\mathbf{0.842 \pm 0.034}$	$\mathbf{0.75 \pm 0.247}$	$\mathbf{0.875 \pm 0.079}$	$\mathbf{0.892 \pm 0.09}$

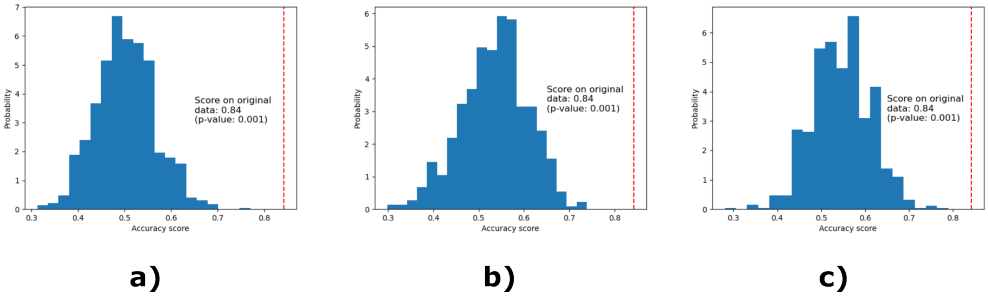

Figure 13. Permutation test with the best results of cross-validation. a) 4.8Hz. b) 16Hz. c) 40Hz.

cesses. In Fig. 10 we show the profiles of six global network measures, where we can draw differences between the real functional brain networks from the fNIRS signals and the equivalent random networks. Small-world organization is a widespread behavior in networks from complex systems, and this is also found in functional brain networks.[43] Fig. 10.c depicts the small-worldness of controls and dyslexics for the three stimuli, where we can observe values greater than one for the small-worldness of control group except for the 40Hz stimuli. The dyslexic group has a deficit of small-worldness value for 4.8Hz and 16Hz. This reduction in the small-worldness of functional brain networks may correspond to a loss of efficient communication over time between distributed brain regions.

Despite these drops, network topology is closely related to small-world organization showing a compromise between functional segregation and integration. Controls and dyslexics networks have both

larger transitivity values that matched random networks (Fig. 10.a). This measure is normalized collectively and quantifies the existence of interconnected modules of brain regions that are indicative of segregated neural processing. In addition, functional brain networks in the three stimuli exhibited systematically higher modularity compared to those derived from paired ensemble of random networks (Fig. 10.f). They also show a slightly larger characteristic path length than matched random networks (Fig. 10.b). However, functional paths are less easy to interpret and compute on disconnected networks.[16] Small-world networks are also characterized as systems with global and local efficiency.[45] If brain networks are compared with equivalent random networks, they have similar global information processing efficiency, but more efficient local information processing.[56] Our functional brain networks for control and dyslexic groups have larger local efficiency than the ensemble of random networks (Fig. 10.e), and similar global efficiency (Fig. 10.d).

Among all these results, if we focus on the profiles of controls and dyslexics through time, we can observe patterns of deviation of the mean values of network metrics between each group throughout the development of the hemodynamic response to the stimulus. This also occurs for regional measures as nodal efficiency (Fig. 12), and the clustering coefficient of each node (Fig. 11). Nodal efficiency is larger in the right hemisphere for control and dyslexics in the three stimuli. This indicates that there are highly integrated areas where specialized information is combined from distributed brain regions. The difference in nodal efficiency between controls and dyslexics is increased for the 40Hz stimulus, in the line of Ref. 10 that have found and a rightward lateralization for high frequencies. The clustering coefficient is larger for the dyslexic group revealing the necessity of a greater number densely interconnected cortical areas for auditory processing, reflecting an inability to quickly settle in phonological representation.[24] The differences found in the complex networks measures could explain why the SVC is capable of detecting DD using certain networks measures as features for each stimulus. For example, mean values of modularity and local efficiency are distant in the 40Hz stimulus through time.

In the present study, the best classification result was obtained by analyzing Hbr signals. Only for the 4.8Hz stimulus the performance were greater for the HbO signals. Consequently, the main results were presented by analyzing the Hbr signals in 16Hz and 40Hz, and HbO signals in 4.8Hz stimuli. In Ref. 34 we can see that HbO and Hbr signals have been used in a large number of fNIRS studies. Furthermore, Ref. 57, 56, 58 have employed both HbO and HbR signals together with graph theory to characterize functional brain networks, finding that quantitative network measures differ between the different hemoglobin concentration signals. These differences can be explained by variations in SNR in the fNIRS measurement, the effects of artifacts on the hemodynamic response, even differences in the origin of hemodynamic responses of different hemoglobin concentration signals stemming from neural activity. The aforementioned have been investigated in several works to identify the relationship between neuronal activity, BOLD signal from fMRI, and hemoglobin concentrations derived from fNIRS data. Their findings are task specific, and depend on the scope and objective of the work. There is an agreement that temporal variations of the BOLD signal are highly correlated with Hbr,[59,60] and increased cerebral blood flow results in a decrement in Hbr and a rise in HbO. However, Ref. 61 come to the needed of new studies to explore the transients of the BOLD signal. Ref. 62 demostrated that the cortical content of the motor cortex fNIRS signal is more present in total hemoglobin concentration than in HbO and Hbr. In contrast, Ref. 63 found stronger functional correlations in HbO and Hbr, but noisier and less localized with total hemoglobin. Finally, Ref. 64 evinced that veins draining the scalp while performing a task induce artifacts in the hemodynamic response of fNIRS signals, affecting more changes in HbO than in Hbr.

5. Conclusions

In this work, we propose a methodology to figure out differential patterns in brain network dynamics, measuring the evolution of the hemodynamic response at different brain areas while an auditory, non-interactive and slow-variation stimulus is presented. Correlation among areas in the hemodynamic response measured by means of HbO and HbR allows to construct a network that is represented as a graph. Then, complex network analysis methodology is used to characterize the graphs, and to extract features

that 1) provide exploratory information to dive into the brain processes related to low-level language processing and 2) provide discriminative information allowing to differentiate between controls and DD subjects. Following the proposed methodology, we found that the topological organization in functional brain networks of control and dyslexic children has the potential to be a diagnostic biomarker for developmental dyslexia. These fluctuations in the networks have been analyzed in the course of an experiment in which children were presented non-speech auditory stimuli. Using an approach in which fNIRS data and complex network analysis are combined, which is largely unexplored in the literature for dyslexia diagnosis.

Of the three stimuli, the phonemic stimulus (40Hz) was the best performing in classification. We have used network measures of functional connectivity in Hbr signals as features to train a SVC, achieving and AUC of 0.89 in differential diagnosis of DD. Complex network analysis also provides measures that quantify the properties of functional brain networks. This can be interpreted to obtain information about the relationship between brain regions in the auditory processing of typical and dyslexic readers.

Acknowledgments

This work was supported by projects PGC2018-098813-B-C32 (Spanish "Ministerio de Ciencia, Innovación y Universidades"), UMA20-FEDERJA-086 and P18-RT-1624 (Consejería de economía y conocimiento, Junta de Andalucía), and by European Regional Development Funds (ERDF) as well as the BioSiP (TIC-251) research group. We gratefully acknowledge the support of NVIDIA Corporation with the donation of one of the GPUs used for this research. Work by F.J.M.M. was supported by the IJC2019-038835-I MICINN "Juan de la Cierva - Incorporación" Fellowship. We also thank the *Leeduca* research group and Junta de Andalucía for the data supplied and support.

Bibliography

1. R. L. Peterson and B. F. Pennington, Developmental dyslexia, *The Lancet* **379** (May 2012) 1997–2007.
2. J. C. Ziegler and U. Goswami, Reading Acquisition, Developmental Dyslexia, and Skilled Reading Across Languages: A Psycholinguistic Grain Size Theory., *Psychological Bulletin* **131**(1) (20050103) p. 3.
3. P. A. Thompson, C. Hulme, H. M. Nash, D. Gooch, E. Hayiou-Thomas and M. J. Snowling, Developmental dyslexia: Predicting individual risk, *J Child Psychol Psychiatr* **56** (September 2015) 976–987.
4. M. J. Snowling, Specific Disorders and Broader Phenotypes: The Case of Dyslexia, *Quarterly Journal of Experimental Psychology* **61** (January 2008) 142–156.
5. I. Kovelman, E. S. Norton, J. A. Christodoulou, N. Gaab, D. A. Lieberman, C. Triantafyllou, M. Wolf, S. Whitfield-Gabrieli and J. D. E. Gabrieli, Brain Basis of Phonological Awareness for Spoken Language in Children and Its Disruption in Dyslexia, *Cerebral Cortex* **22** (April 2012) 754–764.
6. H. Park, R. A. A. Ince, P. G. Schyns, G. Thut and J. Gross, Frontal Top-Down Signals Increase Coupling of Auditory Low-Frequency Oscillations to Continuous Speech in Human Listeners, *Current Biology* **25** (June 2015) 1649–1653.
7. U. Goswami, A temporal sampling framework for developmental dyslexia, *Trends in Cognitive Sciences* **15** (January 2011) 3–10.
8. U. Goswami, A Neural Basis for Phonological Awareness? An Oscillatory Temporal-Sampling Perspective, *Curr Dir Psychol Sci* **27** (February 2018) 56–63.
9. F. J. Martinez-Murcia, A. Ortiz, J. M. Gorriz, J. Ramirez, P. J. Lopez-Abarejo, M. Lopez-Zamora and J. L. Luque, EEG Connectivity Analysis Using Denoising Autoencoders for the Detection of Dyslexia, *Int. J. Neur. Syst.* **30** (July 2020) p. 2050037.
10. M. Lizarazu, M. Lallier, N. Molinaro, M. Bourguignon, P. M. Paz-Alonso, G. Lerma-Usabiaga and M. Carreiras, Developmental evaluation of atypical auditory sampling in dyslexia: Functional and structural evidence, *Hum Brain Mapp* **36** (September 2015) 4986–5002.
11. N. Molinaro, M. Lizarazu, M. Lallier, M. Bourguignon and M. Carreiras, Out-of-synchrony speech entrainment in developmental dyslexia, *Human Brain Mapping* **37**(8) (2016) 2767–2783.
12. V. Leong and U. Goswami, Acoustic-Emergent Phonology in the Amplitude Envelope of Child-Directed Speech, *PLOS ONE* **10** (December 2015) p. e0144411.
13. A.-L. Giraud and D. Poeppel, Cortical oscillations and speech processing: Emerging computational principles and operations, *Nat Neurosci* **15** (April 2012) 511–517.
14. D. Poeppel, The neuroanatomic and neurophysiological infrastructure for speech and language, *Current Opinion in Neurobiology* **28** (October 2014) 142–149.
15. E. Bullmore and O. Sporns, Complex brain networks: Graph theoretical analysis of structural and functional systems, *Nat Rev Neurosci* **10** (March 2009) 186–198.

16. M. Rubinov and O. Sporns, Complex network measures of brain connectivity: Uses and interpretations, *NeuroImage* **52** (September 2010) 1059–1069.
17. M. Zhang, L. Riecke, G. Fraga-González and M. Bonte, Altered brain network topology during speech tracking in developmental dyslexia, *NeuroImage* **254** (July 2022) p. 119142.
18. G. Fraga González, D. J. A. Smit, M. J. W. van der Molen, J. Tijms, C. J. Stam, E. J. C. de Geus and M. W. van der Molen, EEG Resting State Functional Connectivity in Adult Dyslexics Using Phase Lag Index and Graph Analysis, *Frontiers in Human Neuroscience* **12** (2018).
19. G. Fraga González, M. J. W. Van der Molen, G. Žarić, M. Bonte, J. Tijms, L. Blomert, C. J. Stam and M. W. Van der Molen, Graph analysis of EEG resting state functional networks in dyslexic readers, *Clinical Neurophysiology* **127** (September 2016) 3165–3175.
20. G. Fraga-González, D. J. A. Smit, M. J. W. Van der Molen, J. Tijms, C. J. Stam, E. J. C. de Geus and M. W. Van der Molen, Graph Analysis of EEG Functional Connectivity Networks During a Letter-Speech Sound Binding Task in Adult Dyslexics, *Frontiers in Psychology* **12** (2021) p. 5344.
21. T. Taskov and J. Dushanova, Functional Connectivity in Developmental Dyslexia during Speed Discrimination, *Symmetry* **13** (May 2021) p. 749.
22. K. Mandke, S. Flanagan, A. Macfarlane, F. Gabrielczyk, A. Wilson, J. Gross and U. Goswami, Neural sampling of the speech signal at different timescales by children with dyslexia, *NeuroImage* **253** (June 2022) p. 119077.
23. E. S. Finn, X. Shen, J. M. Holahan, D. Scheinost, C. Lacadie, X. Papademetris, S. E. Shaywitz, B. A. Shaywitz and R. T. Constable, Disruption of Functional Networks in Dyslexia: A Whole-Brain, Data-Driven Analysis of Connectivity, *Biological Psychiatry* **76** (September 2014) 397–404.
24. E. S. Edwards, K. Burke, J. R. Booth and C. McNorgan, Dyslexia on a continuum: A complex network approach, *PLOS ONE* **13** (December 2018) p. e0208923.
25. N. J. Gallego-Molina, A. Ortiz, F. J. Martínez-Murcia, M. A. Formoso and A. Giménez, Complex network modeling of EEG band coupling in dyslexia: An exploratory analysis of auditory processing and diagnosis, *Knowledge-Based Systems* **240** (March 2022) p. 108098.
26. J. Wang, Q. Dong and H. Niu, The minimum resting-state fNIRS imaging duration for accurate and stable mapping of brain connectivity network in children, *Sci Rep* **7** (July 2017) p. 6461.
27. J. Gervain, J. Mehler, J. F. Werker, C. A. Nelson, G. Csibra, S. Lloyd-Fox, M. Shukla and R. N. Aslin, Near-infrared spectroscopy: A report from the McDonnell infant methodology consortium, *Developmental Cognitive Neuroscience* **1** (January 2011) 22–46.
28. T. Nguyen, O. Babawale, T. Kim, H. J. Jo, H. Liu and J. G. Kim, Exploring brain functional connectivity in rest and sleep states: A fNIRS study, *Sci Rep* **8** (November 2018) p. 16144.
29. Z. Einalou, K. Maghooli, S. K. Setarehdan and A. Akin, Graph theoretical approach to functional connectivity in prefrontal cortex via fNIRS, *Neurophotonics* **4** (October 2017) p. 041407.
30. K. K. Jasińska, L. Shuai, A. N. L. Lau, S. Frost, N. Landi and K. R. Pugh, Functional connectivity in the developing language network in 4-year-old children predicts future reading ability, *Developmental Science* **24**(2) (2021) p. e13041.
31. S. Cutini, D. Szűcs, N. Mead, M. Huss and U. Goswami, Atypical right hemisphere response to slow temporal modulations in children with developmental dyslexia, *NeuroImage* **143** (December 2016) 40–49.
32. A. Ortiz, F. J. Martinez-Murcia, J. L. Luque, A. Giménez, R. Morales-Ortega and J. Ortega, Dyslexia Diagnosis by EEG Temporal and Spectral Descriptors: An Anomaly Detection Approach, *Int. J. Neur. Syst.* **30** (July 2020) p. 2050029.
33. A. De Vos, S. Vanvooren, J. Vanderauwera, P. Ghesquière and J. Wouters, A longitudinal study investigating neural processing of speech envelope modulation rates in children with (a family risk for) dyslexia, *Cortex* **93** (August 2017) 206–219.
34. L. K. Butler, S. Kiran and H. Tager-Flusberg, Functional Near-Infrared Spectroscopy in the Study of Speech and Language Impairment Across the Life Span: A Systematic Review, *Am J Speech Lang Pathol* **29** (August 2020) 1674–1701.
35. A. Gramfort, M. Luessi, E. Larson, D. Engemann, D. Strohmeier, C. Brodbeck, R. Goj, M. Jas, T. Brooks, L. Parkkonen and M. Hämäläinen, MEG and EEG data analysis with MNE-Python, *Frontiers in Neuroscience* **7** (2013).
36. R. Luke, E. D. Larson, M. J. Shader, H. Innes-Brown, L. V. Yper, A. K. C. Lee, P. F. Sowman and D. McAlpine, Analysis methods for measuring passive auditory fNIRS responses generated by a block-design paradigm, *NPh* **8** (May 2021) p. 025008.
37. F. A. Fishburn, R. S. Ludlum, C. J. Vaidya and A. V. Medvedev, Temporal Derivative Distribution Repair (TDDR): A motion correction method for fNIRS, *NeuroImage* **184** (January 2019) 171–179.
38. D. T. Delpy, M. Cope, P. van der Zee, S. Arridge, S. Wray and J. Wyatt, Estimation of optical pathlength through tissue from direct time of flight measurement, *Phys. Med. Biol.* **33** (December 1988) 1433–1442.
39. A. C. Whiteman, H. Santosa, D. F. Chen, S. Perlman and T. Huppert, Investigation of the sensitivity of functional near-infrared spectroscopy brain imaging to anatomical variations in 5- to 11-year-old children, *Neurophotonics* **5** (January 2018) p. 011009.

40. T. Schreiber and A. Schmitz, Surrogate time series, *Physica D: Nonlinear Phenomena* **142** (August 2000) 346–382.
41. S. Boccaletti, V. Latora, Y. Moreno, M. Chavez and D. U. Hwang, Complex networks: Structure and dynamics, *Physics Reports* **424** (February 2006) 175–308.
42. M. E. J. Newman, The Structure and Function of Complex Networks, *SIAM Rev.* **45** (January 2003) 167–256.
43. D. J. Watts and S. H. Strogatz, Collective dynamics of 'small-world' networks, *Nature* **393** (June 1998) 440–442.
44. L.-D. Lord, A. B. Stevner, G. Deco and M. L. Kringelbach, Understanding principles of integration and segregation using whole-brain computational connectomics: Implications for neuropsychiatric disorders, *Phil. Trans. R. Soc. A.* **375** (June 2017) p. 20160283.
45. V. Latora and M. Marchiori, Efficient Behavior of Small-World Networks, *Phys. Rev. Lett.* **87** (October 2001) p. 198701.
46. S. Achard and E. Bullmore, Efficiency and Cost of Economical Brain Functional Networks, *PLOS Computational Biology* **3** (February 2007) p. e17.
47. O. Sporns and C. J. Honey, Small worlds inside big brains, *Proceedings of the National Academy of Sciences* **103** (December 2006) 19219–19220.
48. M. D. Humphries and K. Gurney, Network 'Small-World-Ness': A Quantitative Method for Determining Canonical Network Equivalence, *PLoS ONE* **3** (April 2008) p. e0002051.
49. L. C. Freeman, Centrality in social networks conceptual clarification, *Social Networks* **1** (January 1978) 215–239.
50. M. E. J. Newman, Assortative Mixing in Networks, *Phys. Rev. Lett.* **89** (October 2002) p. 208701.
51. R. Pastor-Satorras, A. Vázquez and A. Vespignani, Dynamical and Correlation Properties of the Internet, *Phys. Rev. Lett.* **87** (November 2001) p. 258701.
52. V. N. Vapnik, *Statistical Learning Theory* (John Wiley & Sons, New York [etc, 1998).
53. S. Maslov and K. Sneppen, Specificity and Stability in Topology of Protein Networks, *Science* **296** (May 2002) 910–913.
54. K. Lehongre, B. Morillon, A.-L. Giraud and F. Ramus, Impaired auditory sampling in dyslexia: Further evidence from combined fMRI and EEG, *Frontiers in Human Neuroscience* **7** (2013).
55. A. J. Power, N. Mead, L. Barnes and U. Goswami, Neural entrainment to rhythmic speech in children with developmental dyslexia, *Front Hum Neurosci* **7** (November 2013) p. 777.
56. L. Cai, Q. Dong and H. Niu, The development of functional network organization in early childhood and early adolescence: A resting-state fNIRS study, *Developmental Cognitive Neuroscience* **30** (April 2018) 223–235.
57. H. Niu, J. Wang, T. Zhao, N. Shu and Y. He, Revealing Topological Organization of Human Brain Functional Networks with Resting-State Functional near Infrared Spectroscopy, *PLOS ONE* **7** (September 2012) p. e45771.
58. H. Niu, Z. Li, X. Liao, J. Wang, T. Zhao, N. Shu, X. Zhao and Y. He, Test-Retest Reliability of Graph Metrics in Functional Brain Networks: A Resting-State fNIRS Study, *PLOS ONE* **8** (September 2013) p. e72425.
59. M. L. Schroeter, T. Kupka, T. Mildner, K. Uludağ and D. Y. von Cramon, Investigating the post-stimulus undershoot of the BOLD signal—a simultaneous fMRI and fNIRS study, *NeuroImage* **30** (April 2006) 349–358.
60. S. Wijeakumar, T. J. Huppert, V. A. Magnotta, A. T. Buss and J. P. Spencer, Validating an image-based fNIRS approach with fMRI and a working memory task, *NeuroImage* **147** (February 2017) 204–218.
61. J. Steinbrink, A. Villringer, F. Kempf, D. Haux, S. Boden and H. Obrig, Illuminating the BOLD signal: Combined fMRI–fNIRS studies, *Magnetic Resonance Imaging* **24** (May 2006) 495–505.
62. L. Gagnon, M. A. Yücel, M. Dehaes, R. J. Cooper, K. L. Perdue, J. Selb, T. J. Huppert, R. D. Hoge and D. A. Boas, Quantification of the cortical contribution to the NIRS signal over the motor cortex using concurrent NIRS-fMRI measurements, *NeuroImage* **59** (February 2012) 3933–3940.
63. B. R. White, A. Z. Snyder, A. L. Cohen, S. E. Petersen, M. E. Raichle, B. L. Schlaggar and J. P. Culver, Resting-state functional connectivity in the human brain revealed with diffuse optical tomography, *NeuroImage* **47** (August 2009) 148–156.
64. E. Kirilina, A. Jelzow, A. Heine, M. Niessing, H. Wabnitz, R. Brühl, B. Ittermann, A. M. Jacobs and I. Tachtsidis, The physiological origin of task-evoked systemic artefacts in functional near infrared spectroscopy, *NeuroImage* **61** (May 2012) 70–81.